



A mathematical model for efficient extraction of key locations from point-cloud data in track area

Shuyue Chen^{1,7} · Jiaolv Wu^{2,3} · Jian Lu^{1,4} · Xizhao Wang^{5,6}

Received: 11 May 2023 / Accepted: 24 July 2023
© The Author(s) 2023

Abstract

During the construction of a metro system, it is inevitable that deviations will occur between the excavated tunnel and the original designed scheme. As such, it is necessary to adjust the designed scheme to accommodate these discrepancies. Specifically, the adjustment of the designed scheme involves a rigorous process of repeatedly selecting and verifying the feasibility of the proposed modifications using point-cloud data obtained from the tunnel. However, this process can be considerably time-consuming due to the large-scale and potentially redundant nature of the point-cloud data. This paper proposes a mathematical model for point-cloud data acquired in measuring a mined tunnel, which may deviate from the originally designed one. The modeling, which mainly includes determining its normal plane, and building the equation of tunnel point-cloud data, is to quickly extract several key locations in the tunnel surface for modifying the original design in order to achieve a minimum error between the modified design and the mined tunnel. In comparison with the conventional processing of extracting several key locations directly from point-cloud data, our model shows a significant promotion of extraction efficiency under an acceptable error bound. The model is tested in a real tunnel point-cloud data and the testing results confirm the increase of fitting accuracy and the decrease of computational load.

Keywords Point-cloud data · Cylinder equation · Gradient descent

1 Introduction

Metro is an important symbol of modern civilization in a city, which plays an irreplaceable role in easing the traffic jam. Tunnel excavation is the most basic part of metro construction, and its excavation error is usually inevitable

[1]. As shown in Fig. 1, this error refers to the inconsistency between the excavation tunnel and the designed tunnel, which is usually caused by factors such as the complexity of geological conditions, measurement errors and operating errors of Tunnel Boring Machines (TBM). Adjusting the real tunnel to fit the designed scheme would require excavating and reconstructing the tunnel, which may indeed be economically and time-wise impractical in a real-world engineering project. One potential alternative could be to revise

Shuyue Chen, Jiaolv Wu and Jian Lu contributed equally to this work.

✉ Xizhao Wang
xizhaowang@ieee.org

Shuyue Chen
chenshuyue2020@email.szu.edu.cn

Jiaolv Wu
wujiaolv@stu.hqu.edu.cn

Jian Lu
jianlu@szu.edu.cn

¹ College of Mathematics and Statistics, Shenzhen University, Shenzhen, China

² Shenzhen No. 3 Vocational School of Technology, Shenzhen, China

³ College of Engineering, Huaqiao University, Quanzhou, China

⁴ Shenzhen Key Lab. of Advanced Machine Learning and Applications, Shenzhen University, Shenzhen, China

⁵ Guangdong Key Lab. of Intelligent Information Process, Shenzhen University, Shenzhen, China

⁶ College of Computer Science and Software Engineering, Shenzhen University, Shenzhen, China

⁷ School of Software Engineering, Shenzhen Institute of Information Technology, Shenzhen, China

the designed scheme so that it is more compatible with the existing tunnel.

Making adjustments to a designed scheme requires laser scanning or photogrammetry to create a detailed 3D point

cloud model of the real tunnel [2]. This model can then be compared to the original design using specialized software that can overlay the two models and highlight any differences or discrepancies [3–5]. In Fig. 2, an overlapping model

Fig. 1 The diagram illustrates the discrepancy between the designed metro excavation line (represented by the red solid line) and the real excavation line (represented by the yellow solid line)

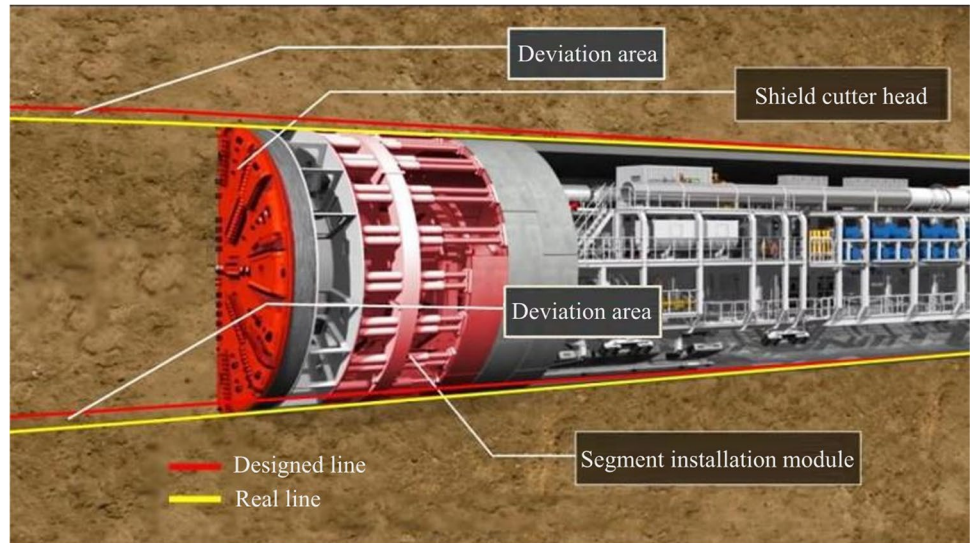


Fig. 2 The overlapping model of a real tunnel comprises a purple model depicting the actual tunnel and a green model depicting the designed tunnel

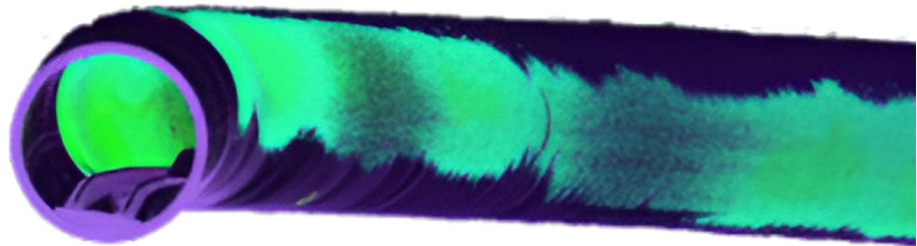


Table 1 The coordinates of the key locations on the base coordinate system, which are provided to the designer to adjust the designed scheme

Tunnel cross-section survey of Shenzhen Metro Line 9 Project							
	Real section				Real measured		
	Left		Right		Top (m)	Bottom (m)	Height (m)
	L (mm)	H (m)	L (mm)	H (m)			
– 1580.238							
Top	2106	– 8.152	2183	– 8.153	– 7.121	– 12.511	5.390
Mid-1	2664	– 9.752	2758	– 9.753			
Mid-2	2551	– 10.622	2637	– 10.624			
Bottom	2292	– 11.201	2388	– 11.202			
– 1575.746							
Top	2077	– 8.224	2181	– 8.229	– 7.199	– 12.597	5.398
Mid-1	2659	– 9.826	2759	– 9.828			
Mid-2	2543	– 10.695	2639	– 10.697			
Bottom	2289	– 11.276	2387	– 11.278			

Project location: 9112-4 Hi-Tech South—Hongshuwan South

Tunnel type: circle tunnel

Measurement time: September 29, 2018, September 30, 2018, October 2, 2018

of a real tunnel is depicted. Despite being possible to visually estimate the size and area of excavation errors, practical engineering typically requires a more rigorous approach. To assess the excavation error of the tunnel quantitatively and qualitatively, designers are provided with a table of key locations coordinates extracted from the tunnel's point-cloud data. Table 1 gives an instance of the key locations, which are selected at intervals and from each cross-section of the tunnel. By comparing the key location coordinates with the relevant thresholds of corresponding positions, it is possible to determine the extent and magnitude of excavation errors in terms of the affected area and size.

On the other hand, point-cloud data may lead to a significant challenge due to its disordered nature, particularly when dealing with large-scale datasets [6]. Extracting the key locations from this data can be a complex and time-consuming task that demands a significant amount of computational resources. Making adjustments to the designed scheme can be equally challenging, as it often requires re-confirming the coordinates of key locations based on the newly designed scheme. This process can be highly error-prone, especially when dealing with complex point-cloud data, leading to a significant amount of wasted time and effort. Therefore, developing a mathematical model that can quickly extract the key location coordinates significantly reduce the time spent on adjusting the designed scheme. This can lead to faster and more efficient design iterations, allowing designers to explore a wider range of design options in less time. Moreover, the ability to quickly extract key location coordinates also enables the use of evolutionary algorithms in the designed process [7]. Evolutionary algorithms rely on evaluating the fitness of a large number of potential solutions, which can be time-consuming when using traditional methods. However, with a model that can quickly extract key location coordinates, the fitness of a newly designed scheme can be evaluated much more quickly, allowing evolutionary algorithms to be used to explore a much larger search space of designed options.

In the past decades, scholars have proposed a lot of modeling methods of tunnel point cloud. Hamid chakeri took the lead in applying point-cloud data to tunnel deformation monitoring [8]. Rinskevan gosliga built the cylindrical model, and then adopted the statistical test method to carry out the tunnel deformation monitoring [9]. Fekete diderichs and Lato adopted the triangular mesh method to model the tunnel [10]. All of the above studies were aimed at simulating the real tunnel through the point-cloud data processing [11, 12], splicing [13], and 3D reconstruction [14]. Despite the fact that these methods are capable of accurately representing the shape of a real tunnel, they are currently impractical for efficiently adjusting the designed scheme, as this process often involves repeatedly extracting key location coordinates, which can be time-consuming. Moreover, the

modeling techniques discussed above exclusively pertain to modeling tunnels that have been completed post-construction. Consequently, these approaches are inapplicable to tunnels that have not undergone track installation.

This paper proposes a mathematical model that aims to extract key location coordinates from point-cloud data quickly. The model consists of several steps: firstly, the gradient descent method is used to extract the point-cloud belonging to the same cross-section from the point-cloud data. Then, the least square method [15, 16] is applied to calculate the center point of each cross-section. Subsequently, a tunnel centerline composed of multiple polylines is obtained by connecting the center point of the adjacent cross-sections. Finally, the paper proposes a tunnel model based on the centerline and provides a method for extracting key position coordinates from this model. The proposed model is tested in a real metro tunnel, and the comprehensive experiment shows that it effectively reduces the extraction time of key location coordinates while ensuring that the deviation between the proposed model and the tunnel point-cloud data is within an acceptable range.

The remaining of this paper includes the following sections: Sect. 2 provides the related work. Section 3 presents the construction process of our model. Section 4 shows an experimental test on a real data set and discussions of the results. And Sect. 5 concludes this paper.

2 Preliminaries

2.1 Tunnel clearance and base coordinate

Tunnel clearance is a crucial consideration in the design and construction of metro systems to ensure that trains can travel safely without colliding with tunnel walls or obstacles [17, 18]. As shown in Fig. 3, various gauges are involved in this process, including the metro profile, which encompasses the maximum dimensions of the train when in motion. The equipment gauge pertains to the required space for installing signaling equipment, power cables, ventilation systems, and other equipment along the track [19, 20]. The metro gauge accounts for the tunnel's dimensions, including width, height, curvature, and extra space required for equipment installation.

To aid the designers in their endeavor to consider the diverse equipment within the tunnel during the adjustment phase of metro construction, the scanned three-dimensional key location coordinates will be transformed into a two-dimensional coordinate system in the base coordinate framework. The base coordinate framework, as illustrated in Fig. 3, employs the central point of the track as the origin, while the track plane and metro centerline serve as the x -axis and y -axis, respectively.

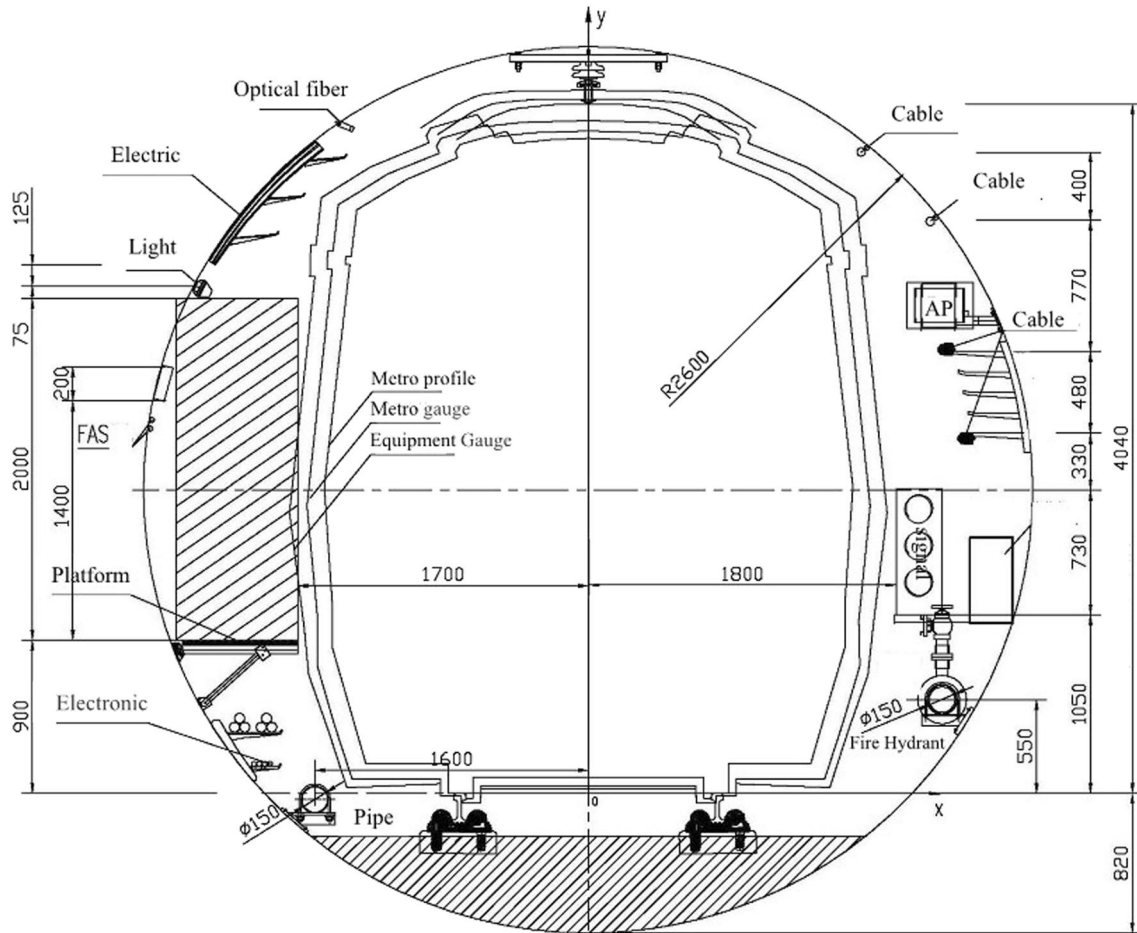


Fig. 3 This figure illustrates the cross-sectional view of the subway tunnel in a schematic form

2.2 Key locations of the tunnel cross-section

Metro tunnel cross-section measurement is the process of precisely scanning the profile of the tunnel cross-section during metro construction to ensure the tunnel clearance has not been violated and to provide a basis for the modifications of the designed scheme. To accurately reflect the profile and size of the metro tunnel cross-section, surveyors place multiple key locations along the cross-section following the designed line. The designers then determine the deviation direction and magnitude of the each cross-section based on the deviation values at key locations of the real tunnel.

Figure 4a describes the key locations of a cross-section. Generally, the key locations can be divided into 4 categories:

- **Top right/left.** These locations can reflect the height and arch shape of the cross-section. The horizontal deviations of these types of key locations are focused on during metro construction.

- **Bottom right/left.** These locations can reflect the depth and planarity of the cross-section. The horizontal deviations of these types of key locations are focused on during metro construction.
- **Mid right/left 1 and mid right/left 2.** These locations can reflect the linearity and slope of the cross-section. The horizontal deviations of these types of key locations are focused on during metro construction.
- **Top and bottom.** These locations can reflect the width and curvature of the cross-section. The vertical deviations of these types of key locations are focused on during metro construction.

2.3 Intrusion gauge

Figure 4a depicts the theoretical and real cross-sections using a red and blue circle, respectively. The diameter of the real cross-section is slightly larger than that of the design

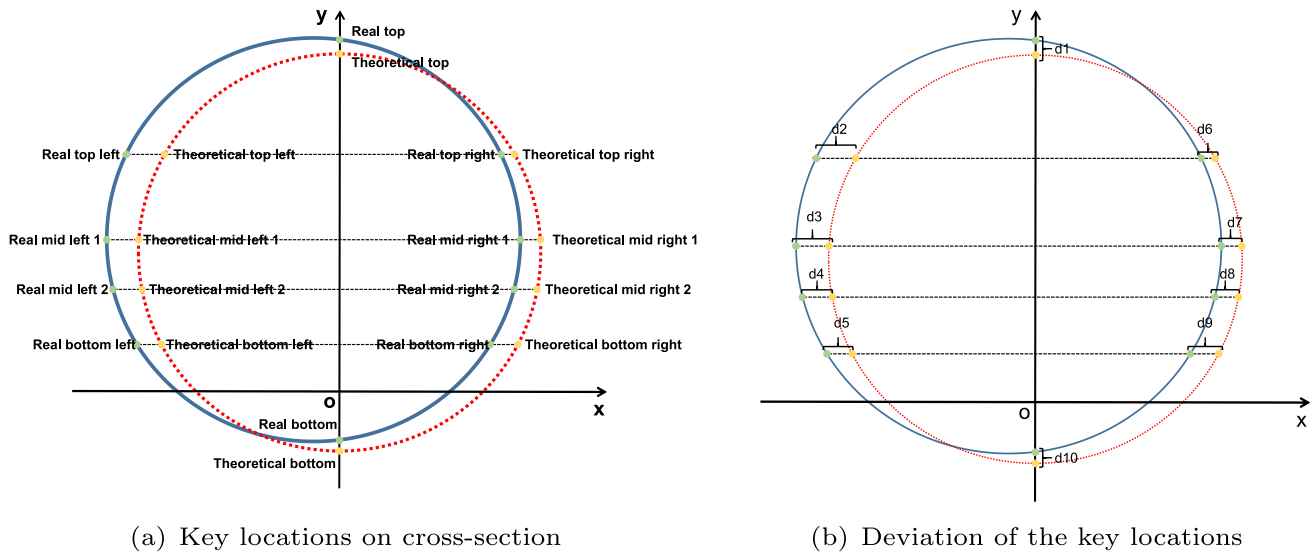


Fig. 4 **a** Presents a schematic diagram illustrating 10 significant locations on a cross-section. **b** Displays the disparity between the designed and actual cross-sections. Notably, the circle outlined with

red dashed lines represents the cross-section of the designed tunnel, whereas the circle outlined with blue solid lines represents the cross-section of the actual tunnel

cross-section to provide adequate adjustment space for the designer. If a theoretical key location falls within the real cross-section, additional space is available for it. Conversely, if a key location falls outside the real cross-section, it is considered violated. Consequently, Fig. 4a shows 5 invasion locations: top right, mid right 1, mid right 2, bottom right, and bottom.

Finally, Fig. 5 illustrates the process in which the designer adjusts the designed scheme to meet the requirements of the real tunnel.

2.4 Adjustment of designed line

3 Methodology

The adjustment of the designed line refers to the process of measuring the three-dimensional structure of a tunnel that has been constructed, and subsequently, optimizing the original design scheme in accordance with the actual conditions on-site. This process enables the necessary adjustments to be made to ensure the requirements of the various equipment within the tunnel are met. Generally, the adjustment of the designed line is a process that enhances the smoothness of the metro tunnel and increases the safety and comfort of driving.

This section presents a novel approach aimed at enhancing the efficiency of metro designed scheme adjustments by constructing a mathematical model of the real tunnel, replacing the conventional method of extracting key locations from the point-cloud data of the metro tunnel. The mathematical model is built upon the geometric properties, structure, and point-cloud data of the tunnel. With a strict adherence to the accuracy requirements, i.e., a deviation not exceeding 2 cm, this method greatly reduces the time required to extract the key locations.

Figure 4b illustrates the deviation between the real and designed tunnel cross-sections. Let C_i be a cross-section containing 10 key locations $\{\kappa_{i,j}\}_{j=1}^{10}$. The deviation of C_i at the 10 key locations is denoted by $\{d_{i,j}\}_{j=1}^{10}$, where $d_{i,j} > 0$ indicates that C_i has additional space $d_{i,j}$ at $\kappa_{i,j}$, while $d_{i,j} < 0$ indicates an intrusion of $-d_{i,j}$ at $\kappa_{i,j}$. The cross-section C_i does not intrude on the equipment gauge if and only if $\forall \kappa_{i,j} \in C_i, d_{i,j} > 0$. Let $\mathbb{C} = \{C_i\}_{i=1}^n$ be the set of measured cross-sections. It follows that the designed tunnel satisfies the design requirements if and only if $\forall C_i \in \mathbb{C}, C_i$ does not intrude on the equipment gauge.

3.1 Problem formulation

Let \mathcal{D} represents the point-cloud data of the real tunnel. During the process of adjusting the designed scheme, several key locations $\mathbb{K} = \{\kappa_{i,j}^{\mathcal{D}}\}$ from the selected cross-sections $\mathbb{C} = \{C_i\}_{i=1}^n$ are extracted to reflect the geometric properties and structure of the real tunnel, where $\{\kappa_{i,j}^{\mathcal{D}}\}_{j=1}^{10}$ denotes the key locations on C_i . This paper aims at constructing a mathematical model \mathcal{M} to approximate the point-cloud data for extracting the key locations. To accurately reflect the shape of the real tunnel, the deviations between the key locations $\{\kappa_{i,j}^{\mathcal{D}}\}$ extracted from \mathcal{D} and the key locations $\{\kappa_{i,j}^{\mathcal{M}}\}$ extracted

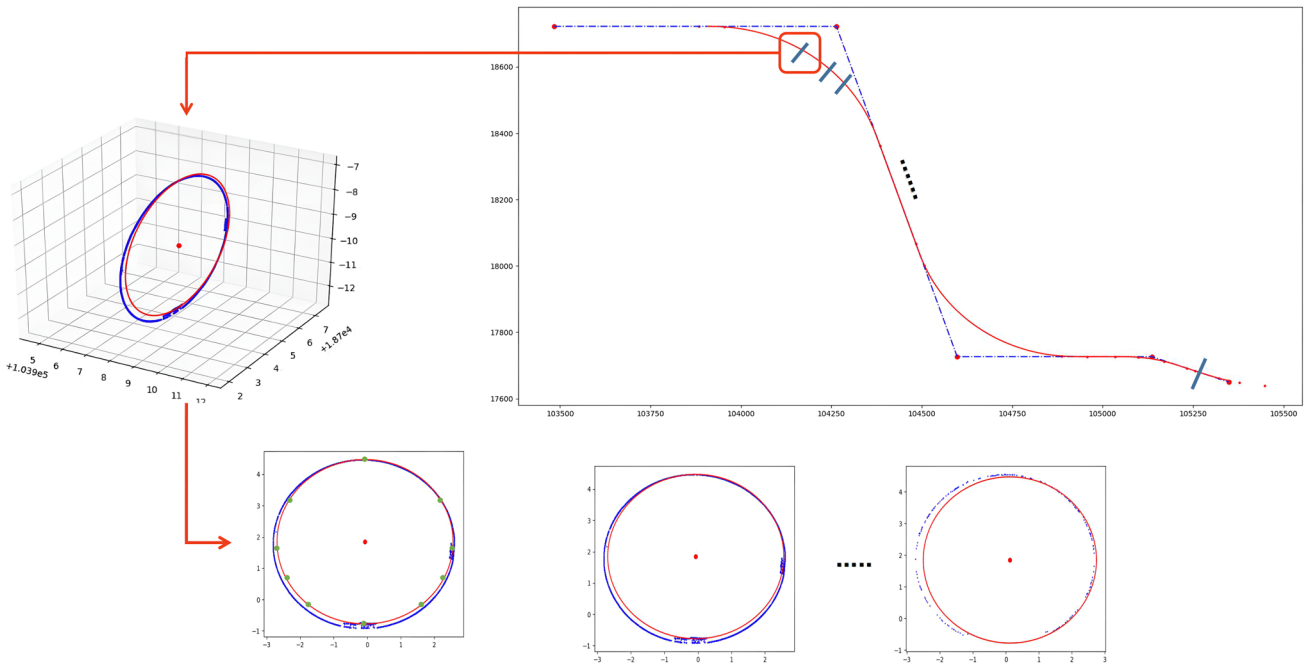


Fig. 5 Schematic diagram of the process of the designer adjusting the design tunnel. Several cross-sections are scanned at fixed distance intervals. For each cross-section, the circle with red solid lines represents the designed cross-section, while the blue scattered points rep-

resent the point cloud of the scanned actual cross-section. In theory, a feasible design tunnel must ensure that all the designed cross-sections are within the actual cross-sections

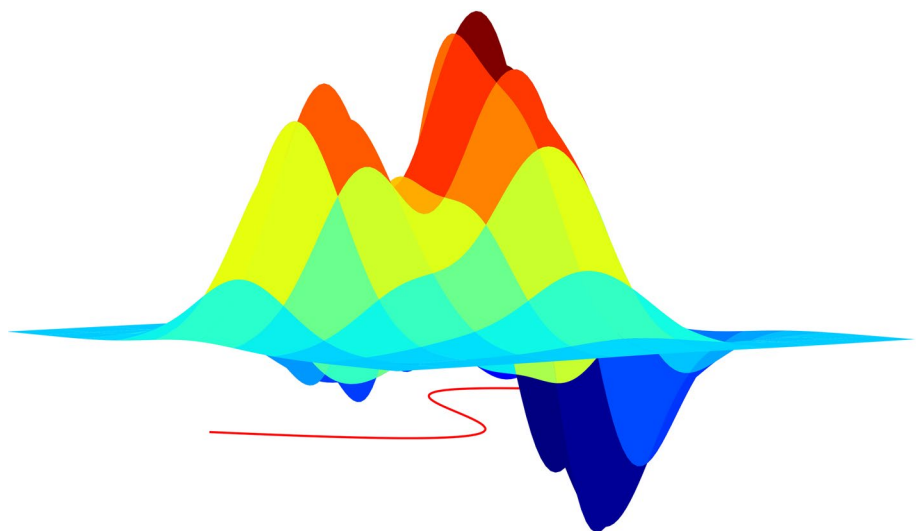
from \mathcal{M} must satisfy the condition that $\text{dis}(\kappa_{ij}^D, \kappa_{ij}^M) < 2 \text{ cm}$, where $\text{dis}(\cdot, \cdot)$ is the distance function that measures the Euclidean distance between κ_{ij}^D and κ_{ij}^M .

3.2 Proposed model

In this section, we propose a mathematical model to simulate the real tunnels using multi-segment cylinders. The

proposed model consists of three main steps: extract the real normal plane, constructing the tunnel model, and extracting key positions from mathematical models. Prior to introducing our proposed methodology, it is pertinent to first present a fundamental piece of knowledge. In practical engineering, the construction team is typically furnished with a Computer-Aided Design (CAD) model of the tunnel. This model is constructed based on the line that connects the

Fig. 6 Diagram illustrating the centerline of the route. Formally, the centerline of a route is represented as a curve in a three-dimensional coordinate system



origin of the base coordinate system (route centerline) in the spatial domain. Figure 6 shows an example of the route centerline. Formally, the equation of the route centerline can be expressed as Eq. (1):

$$(o_1, o_2, o_3) = f(s), \tag{1}$$

The symbol s represents the distance from the starting point of the tunnel on the designated line and the coordinate of the origin of the base coordinate system of the cross-section C_s at the location corresponding to the mileage s is given by (o_1, o_2, o_3) . It should be noted that the formula for the route centerline, known as Eq. (1), is integrated within CAD software. The exact structure of this formula is outlined in the appropriate materials.

3.2.1 The extraction of the normal plane

Given Eq. (1), the direction vector v can be approximately expressed as Eq. (2):

$$v = \frac{f(s + \tau) - f(s - \tau)}{2\tau}, \tag{2}$$

where τ is a constant, which is set to 0.01 in our experiment and f represents Eq. (1).

Supposed the direction vector in C_s is (A_s, B_s, C_s) , the point-cloud data of the cross-section on C_s satisfies Eq. (3):

$$A_s x + B_s y + C_s z - (A_s o_1 + B_s o_2 + C_s o_3) = 0. \tag{3}$$

Given the point-cloud data \mathcal{D} , we can extract the point-cloud data $\mathcal{D}_s = \{(X_i, Y_i, Z_i)\}_{i=1}^t$ of the cross-section at mileage s based on Eq. (3), where t is the number of the point-cloud data. It is important to mention that the cross-section referred to here is derived from the designated line, rather than the real tunnel cross-section. Therefore, the shape of the cross-section profile is elliptical.

As previously mentioned, the base coordinate system is a two-dimensional coordinate system. Therefore, it is possible to transform \mathcal{D}_s into this two-dimensional coordinate system. In terms of spectral properties, Eq. (4) defines the x -axis and y -axis of the base coordinate system on C_s :

$$\begin{cases} i' = \left(\frac{B_s(o_2 + 1) + C_s o_3 + D}{A_s} - o_1 \ 1 \ 0 \right), \\ j' = (A_s \ B_s \ C_s) \times i'. \end{cases} \tag{4}$$

where i' and j' are the direction vectors of x -axis and y -axis, $D = -(A_s o_1 + B_s o_2 + C_s o_3)$.

Then, the coordinate of the point-cloud data on the two-dimensional coordinate system can be written as:

$$\begin{pmatrix} x \\ y \end{pmatrix} = \begin{pmatrix} i_1 & j_1 \\ i_2 & j_2 \\ i_3 & j_3 \end{pmatrix}^{-1} \left(\begin{pmatrix} X \\ Y \\ Z \end{pmatrix} - \begin{pmatrix} o_1 \\ o_2 \\ o_3 \end{pmatrix} \right), \tag{5}$$

where i_1, i_2, i_3 and j_1, j_2, j_3 are the components of i' and j' , (X, Y, Z) represents the point-cloud data in \mathcal{D}_s and (x, y) represents the coordinate of (X, Y, Z) after coordinate conversion.

A circle on the designed normal plane will be fitted by using the least square method.

Let

$$\begin{cases} C' = t \sum_{i=1}^t x_i^2 - \left(\sum_{i=1}^t x_i \right)^2, \\ D' = t \sum_{i=1}^t x_i y_i - \sum_{i=1}^t x_i \sum_{i=1}^t y_i, \\ E' = t \sum_{i=1}^t x_i^3 + t \sum_{i=1}^t x_i y_i^2 - \sum_{i=1}^t (x_i^2 + y_i^2) \sum_{i=1}^t x_i, \\ G' = t \sum_{i=1}^t y_i^3 - \left(\sum_{i=1}^t y_i \right)^2, \\ H' = t \sum_{i=1}^t x_i^2 y_i + t \sum_{i=1}^t y_i^3 - \sum_{i=1}^t (x_i^2 + y_i^2) \sum_{i=1}^t y_i, \end{cases} \tag{6}$$

where (x_i, y_i) are the coordinates of the point-cloud data \mathcal{D}_s after coordinate conversion.

Then the center (a, b) of the fitted circle can be derived according to Eq. (7):

$$\begin{cases} a = \frac{H'D' - E'G'}{2(D'^2 - C'G')}, \\ b = \frac{H'C' - E'D'}{2(D'^2 - C'G')}. \end{cases} \tag{7}$$

Let

$$c = -\frac{\sum_{i=1}^t (x_i^2 + y_i^2) + a \sum_{i=1}^t x_i + b \sum_{i=1}^t y_i}{t}. \tag{8}$$

Then, the radius R , of the fitted circle can be derived according to Eq. (9):

$$R = \frac{1}{2} \sqrt{a^2 + b^2 - 4c}. \tag{9}$$

Algorithm 1 Extracting the real normal plane

Input: Point-cloud data \mathcal{D} , the mileage of the extracted normal plane s .

Output: The parameters A^*, B^*, C^* of the real normal plane.

- 1: Calculate the initial cross-section parameters A_s, B_s, C_s according to eq.(2);
 - 2: **for** $i \leftarrow 1 \dots T$ **do**
 - 3: Obtain point-cloud data \mathcal{D}_s in \mathcal{D} that satisfies eq.(3);
 - 4: Calculate the *loss* of based on eq.(12);
 - 5: Calculate the gradients $\frac{\partial loss}{\partial A_s}, \frac{\partial loss}{\partial B_s}$ and $\frac{\partial loss}{\partial C_s}$ of the parameters of \mathcal{C}_s ;
 - 6: Update A_s, B_s, C_s according to $\frac{\partial loss}{\partial A_s}, \frac{\partial loss}{\partial B_s}$ and $\frac{\partial loss}{\partial C_s}$ based on gradient descent method;
 - 7: **if** $A^* - A_s < \eta$ or $B^* - B_s < \eta$ or $C^* - C_s < \eta$ and $i \neq 0$ **then**
 - 8: break;
 - 9: **end if**
 - 10: $A^* \leftarrow A_s, B^* \leftarrow B_s, C^* \leftarrow C_s$;
 - 11: **end for**
 - 12: **return** A^*, B^*, C^* .
-

Therefore, the equation of the fitting cycle can be written as Eq. (10):

$$R^2 = (x - a)^2 + (y - b)^2. \tag{10}$$

As the previous step involved fitting an elliptical point-cloud data to a circle, it is possible to derive a loss function Eq. (11) representing the deviation between the designed cross-section and the real normal plane, as follows:

$$loss = \sum_{i=1}^t ((x_i - a)^2 + (y_i - b)^2 - R^2)^2. \tag{11}$$

The loss function Eq. (12) between $A', B', C', \mathcal{D}_s$ and *loss* can be derived by combining Eqs. (3–11):

$$loss = F(A_s, B_s, C_s, \mathcal{D}_s), \tag{12}$$

where F is the loss function between A_s, B_s, C_s and *loss*.

Finally, we propose to use the gradient descent method to minimize the *loss* and obtain the parameters (A^*, B^*, C^*) of the real normal plane. Algorithm 1 provides a comprehensive breakdown of the process for extracting the real normal plane.

3.2.2 Constructing the tunnel model

By utilizing Eqs. (1–7), one can obtain a set of center points, denoted by $P = (a_0, b_0), (a_1, b_1), \dots, (a_n, b_n)$, by fitting the center of each normal plane. The value of n depends on the

distance between the designed line and the adjacent cross-sections. One can construct a polyline in the three-dimensional coordinate system by connecting the neighboring center points in P . Prior to connecting the center points, it is necessary to transform each center point to its corresponding three-dimensional coordinate using Eq. (13):

$$(\hat{a}_i, \hat{b}_i, \hat{c}_i) = a_i \times i' + b_i \times j' + (o_1, o_2, o_3). \tag{13}$$

This polyline can be used to construct several cylinders, which can replace the point-cloud data of the real tunnel.

The equation of a cylinder can be expressed as follows:

$$(X - a)^2 + (Y - b)^2 + (Z - c)^2 = R^2, \tag{14a}$$

$$P_1X + P_2Y + P_3Z + D = 0, \tag{14b}$$

$$P_1a + P_2b + P_3c + D = 0. \tag{14c}$$

$$\frac{a - \alpha}{P_1} = \frac{b - \beta}{P_2} = \frac{c - \gamma}{P_3}. \tag{14d}$$

The variables a, b, c , and D are accompanied by the constants (P_1, P_2, P_3) and (α, β, γ) , where $(P_1, P_2, P_3) = (\hat{a}_{i+1}, \hat{b}_{i+1}, \hat{c}_{i+1}) - (\hat{a}_i, \hat{b}_i, \hat{c}_i)$ denotes the directional vector of the cylinder's central axis and (α, β, γ) represents a point on the central axis.

Equation (15) can be obtained by combining Eq. (14c) and Eq. (14d):

$$\begin{pmatrix} a \\ b \\ c \end{pmatrix} = M^{-1} \begin{pmatrix} \varepsilon \\ \xi \\ -D \end{pmatrix}, \tag{15}$$

where $M = \begin{pmatrix} P_2 & -P_1 & 0 \\ P_3 & 0 & -P_1 \\ P_1 & P_2 & P_3 \end{pmatrix}$, $\varepsilon = \alpha P_2 - \beta P_1$, and

$\xi = \alpha P_3 - \gamma P_1$.
Let

$$M^{-1} = \begin{pmatrix} m_{11} & m_{12} & m_{13} \\ m_{21} & m_{22} & m_{23} \\ m_{31} & m_{32} & m_{33} \end{pmatrix}.$$

Then Eq. (15) can be converted to Eq. (16):

$$\begin{cases} a = p_1 - q_1 D \\ b = p_2 - q_2 D, \\ c = p_3 - q_3 D \end{cases} \tag{16}$$

where $\begin{cases} p_1 = m_{11}\varepsilon + m_{12}\xi, \\ p_2 = m_{21}\varepsilon + m_{22}\xi, \\ p_3 = m_{31}\varepsilon + m_{32}\xi, \\ q_1 = m_{13}, \\ q_2 = m_{23}, \\ q_3 = m_{33}. \end{cases}$ Then, Eq. (16) can be written as

Eq. (17):

$$\begin{cases} (X - a)^2 = (X \ Y \ Z) N_1 (X \ Y \ Z)^T - 2p_1 (X \ Y \ Z) W_1 + p_1^2 \\ (Y - b)^2 = (X \ Y \ Z) N_2 (X \ Y \ Z)^T - 2p_2 (X \ Y \ Z) W_2 + p_2^2, \\ (Z - c)^2 = (X \ Y \ Z) N_3 (X \ Y \ Z)^T - 2p_3 (X \ Y \ Z) W_3 + p_3^2 \end{cases} \tag{17}$$

where $\begin{cases} N_1 = \begin{pmatrix} (1 - q_1 P_1)^2 & -(1 - q_1 P_1) q_1 P_2 & -(1 - q_1 P_1) q_1 P_3 \\ -(1 - q_1 P_1) q_1 P_2 & (q_1 P_2)^2 & q_1 P_2 q_1 P_3 \\ -(1 - q_1 P_1) q_1 P_3 & q_1 P_2 q_1 P_3 & (q_1 P_3)^2 \end{pmatrix}, \\ N_2 = \begin{pmatrix} (q_2 P_1)^2 & -q_2 P_1 (1 - q_2 P_2) & q_2 P_1 q_2 P_3 \\ -q_2 P_1 (1 - q_2 P_2) & (1 - q_2 P_2)^2 & -(1 - q_2 P_2) q_2 P_3 \\ q_2 P_1 q_2 P_3 & -(1 - q_2 P_2) q_2 P_3 & (q_2 P_3)^2 \end{pmatrix}, \\ N_3 = \begin{pmatrix} (q_3 P_1)^2 & q_3 P_1 q_3 P_2 & -q_3 P_1 (1 - q_3 P_3) \\ q_3 P_1 q_3 P_2 & (q_3 P_2)^2 & -q_3 P_2 (1 - q_3 P_3) \\ -q_3 P_1 (1 - q_3 P_3) & -q_3 P_2 (1 - q_3 P_3) & (1 - q_3 P_3)^2 \end{pmatrix}, \\ W_1 = \begin{pmatrix} 1 - q_1 P_1 & -q_1 P_2 & -q_1 P_3 \end{pmatrix}^T, \\ W_2 = \begin{pmatrix} -q_2 P_1 & 1 - q_2 P_2 & -q_2 P_3 \end{pmatrix}^T, \\ W_3 = \begin{pmatrix} -q_3 P_1 & -q_3 P_2 & 1 - q_3 P_3 \end{pmatrix}^T. \end{cases}$

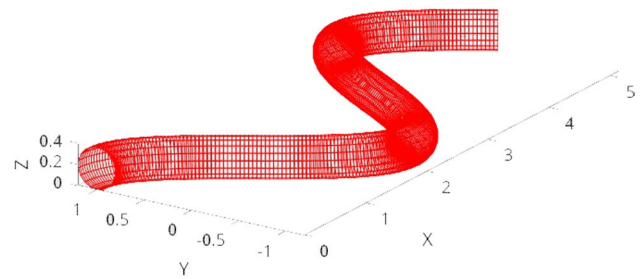


Fig. 7 The proposed mathematical model consists of multiple connected cylindrical segments

Let $\begin{cases} N = N_1 + N_2 + N_3, \\ W = -2p_1 W_1 - 2p_2 W_2 - 2p_3 W_3. \end{cases}$ Finally the cylinder can be expressed as Eq. (18):

$$(X \ Y \ Z) N \begin{pmatrix} X \\ Y \\ Z \end{pmatrix} + (X \ Y \ Z) W + E = R^2, \tag{18}$$

where $E = p_1^2 + p_2^2 + p_3^2$. We can derive the expression $F_i(a_i, b_i, a_{i+1}, b_{i+1})$ for the cylinder that has the central axis with endpoints (a_i, b_i) and (a_{i+1}, b_{i+1}) by utilizing Eqs. (13–18).

Formally, the proposed model, which comprises several cylinders, can be written as Eq. (19):

$$\text{Tunnel}(P) = \begin{cases} F_1(a_1, b_1, a_2, b_2), & s_1 \leq s < s_2 \\ F_2(a_2, b_2, a_3, b_3), & s_2 \leq s < s_3 \\ \dots \\ F_{n-1}(a_{n-1}, b_{n-1}, a_n, b_n), & s_{n-1} \leq s < s_n \end{cases}, \tag{19}$$

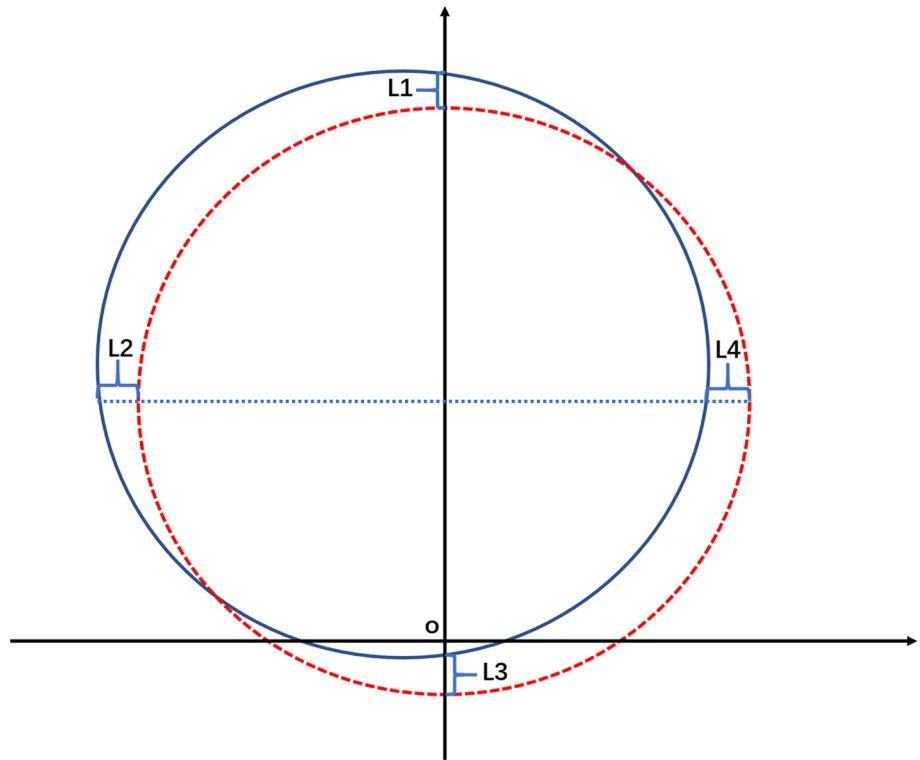
where s_i denotes the mileage of C_i . Figure 7 shows the proposed model, which is replaced with the point-cloud data, to improve the efficiency of the key locations extraction.

3.2.3 Extraction of real cross-section from our model

The deviation of the designed tunnel and the real tunnel will cause the cross-sections of the designed line to be an ellipse. In order to facilitate the measurement of excavation errors, key locations will be extracted based on the base coordinate system, which is mentioned in Sect. 3.2.1. By combining Eqs. (5) and (18), the equation of the ellipse on the two-dimensional coordinate system can be written as Eq. (20):

$$S \begin{pmatrix} x \\ y \end{pmatrix} + (x \ y) T \begin{pmatrix} x \\ y \end{pmatrix} + E_1 = R^2, \tag{20}$$

Fig. 8 The key locations and their corresponding deviations employed in comparative experiments, where the circle with red dashed lines represents the cross-section of the designed tunnel, while the circle with blue solid lines represents the cross-section of the actual tunnel



where

$$\begin{cases} S = (o_1 \ o_2 \ o_3)N \begin{pmatrix} i_1 & j_1 \\ i_2 & j_2 \\ i_3 & j_3 \end{pmatrix} + \left(\begin{pmatrix} i_1 & i_2 & i_3 \\ j_1 & j_2 & j_3 \end{pmatrix} \left(N \begin{pmatrix} o_1 \\ o_2 \\ o_3 \end{pmatrix} + W \right) \right)^T, \\ T = \begin{pmatrix} i_1 & i_2 & i_3 \\ j_1 & j_2 & j_3 \end{pmatrix} N \begin{pmatrix} i_1 & j_1 \\ i_2 & j_2 \\ i_3 & j_3 \end{pmatrix}, \\ E_1 = (o_1 \ o_2 \ o_3)N \begin{pmatrix} o_1 \\ o_2 \\ o_3 \end{pmatrix} + (o_1 \ o_2 \ o_3)W + E. \end{cases}$$

Equation (20) depicts the formula for the cross-section of the real metro tunnel. By plugging in the corresponding elevation value of y into the equation, the coordinate value of x for the key locations can be calculated (Fig. 8).

4 Model testing on real-world point-cloud data

4.1 A real-world point-cloud data set

We conducted an empirical evaluation of the proposed method on a 2 km segment of track located in Shenzhen. The scanning equipment utilized in the evaluation exhibited a maximum distance measurement error of ± 1 mm and

an angular accuracy error of no less than 19 arc seconds (vertical/horizontal angles). Notably, the inter-point distance within the point-cloud data did not exceed 1 cm. The scanning process involved the deployment of a Leica P40 high-precision 3D laser scanner (refer to Fig. 9 for detailed specifications) and subsequent processing of the acquired data using the Cyclone software, specialized for 3D laser point-cloud data. Additionally, an independent station setup was employed during the scanning procedure, as illustrated in Fig. 10. The point-cloud dataset obtained from the tunnel encompassed a substantial 630 million points, resulting in a file size of 28 G. The tunnel exhibited a complex geometry comprising four curves and seven slope variations, with a maximum vertical difference exceeding 10 ms. The construction of an authentic tunnel model based on the point-cloud data offers a reliable means of effectively validating the performance of the proposed method. Finally, the visualization of the point-cloud data is given in Fig. 11.

4.2 Performance indicator

In order to assess the accuracy of our model in relation to the point-cloud data, we employ longitudinal and lateral deviations as experimental metrics. As depicted in Fig. 8, we pinpoint four critical locations within a given cross-section and evaluate the deviation between the model-generated cross-section and the authentic cross-section, utilizing L_1



Parameter	ScanStation P40	Parameter	ScanStation P40
Scan rate	1000,000 Point / second	Dustproof and waterproof (IP)	IP54
Scan angle	360°×270°	Custom scan	Yes
Point surface accuracy	2mm	Model accuracy	2mm
Laser type	class 1	Traditional measurement function	Single point measurement, Traverse measurement
Biaxial compensation	can be turned on / off, resolution ratio 1", compensation range ±5', compensation accuracy 1.5"	Station splicing method	1. Independent station setup, automatic splicing of targets and point clouds; 2. Whole station ceremony, rear view orientation, azimuth setting, rear intersection, automatic splicing
Data storage	256G built-in Solid-state drive + USB 3.0 flash memory	Battery operating time	2 pieces ≥ 7h, Supports hot swapping (uninterruptible power supply)
Scanning distance	300m@18% reflectivity	Weight	11kg
Camera equipment	built in 500w pixel coaxial camera	Scanning method	built in high-definition Chinese touch screen, guided scanning
Operation temperature	-20°C ~ 50°C	Storage temperature	-40°C ~ 70°C

Fig. 9 The parameter of the Leica P40 high-precision 3D laser scanner



Fig. 10 Schematic diagram of independent station setup method

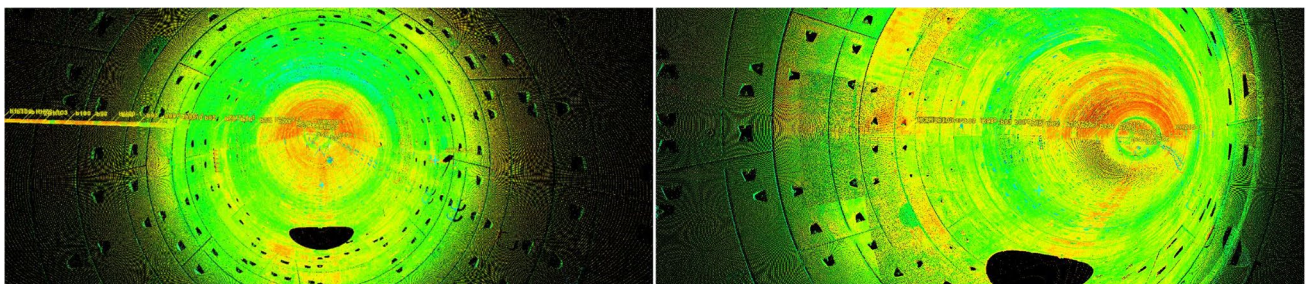


Fig. 11 Visualization of the point cloud collected in the experiment

to L_4 parameters. These locations are carefully selected for their significance in determining the overall shape of the cross-section.

To calculate the deviation at each location, we measure the distance between the corresponding points of the model and point-cloud data along both the longitudinal and lateral directions. This is achieved through the use of appropriate metrics, such as Euclidean distance or absolute difference. The resulting values of L_1 to L_4 parameters allow for

a quantitative assessment of the model’s performance, with a smaller value indicating greater agreement between the model and the point-cloud data.

Taken together, this methodology provides a reliable and objective approach to evaluating the model’s ability to capture the shape of the cross-section, and affords the identification of areas where further refinement may be required.

With respect to our experimental setup, we maintain a mileage distance of 0.1m between successive cross-sections.

For optimization purposes, we implement the gradient descent method with a maximum iteration limit of 5000 and a learning rate of $5e-12$.

4.3 Performance analysis

After conducting experiments on our proposed model, we have extracted 10 cross-sections from various locations of the tunnel. Our model identifies four significant locations for each cross-section, which are then compared with the corresponding key locations of the actual tunnel. The deviation between the two sets of locations is presented in Table 2. The tm column denotes the actual key locations, the om column denotes the key locations extracted from our model, and the dif column represents the difference between the two.

To assess the effectiveness of our proposed model, we analyze the deviation in key locations between the actual tunnel and our model. From Table 2, it is observed that the differences between the actual and extracted key locations vary from -5 to 11.4 mm. The largest deviation of 11.4 mm is observed in the top section of the first cross-section, which is a transition curve. On the other hand, the smallest deviation of 0.1 mm is observed in the mid-left-1 section of the third cross-section, which is also a transition curve. Overall, the key locations extracted by our model are relatively close to the actual key locations, with an average deviation of 2.9 mm and a standard deviation of 3.1 mm.

The model shows promising results in identifying key locations for most of the cross-sections. For instance, the circular curve in the second cross-section has a relatively small deviation of 2.7 mm, indicating a good fit between the model and the actual tunnel. However, the model’s performance is

not as good in some sections. For instance, the top section of the first cross-section has the largest deviation, suggesting that the model needs improvement in identifying key locations for transition curves.

The mean absolute error (MAE) and root mean squared error (RMSE) are calculated to evaluate the performance of the proposed model. The obtained values for MAE and RMSE are 3.64 and 5.17 , respectively. These metrics indicate that the model’s performance is satisfactory. The MAE of 3.64 suggests that the average difference between the predicted and actual values is approximately 3.64 mm. Similarly, the RMSE of 5.17 suggests that there is some level of variance in the model’s predictions.

Finally, a time-complexity analysis is conducted to evaluate the efficiency of our proposed model in extracting key locations from point-cloud data. The results of this analysis are presented in Table 3. The findings demonstrate that our model outperforms the conventional point-cloud data approach in terms of extraction time. This is a notable advantage as it facilitates the efficient utilization of resources and enables the analysis of larger datasets in a shorter period. Therefore, our proposed model offers significant potential for enhancing the accuracy and scalability of location-based applications.

Table 3 Comparing the time taken to extract key locations from point-cloud data versus extracting key locations from the proposed mathematical model

Number of cross-sections	100	500	1000	2500	5000
Time of traditional method [7]	0.704	3.625	7.187	18.318	37.271
Time of our method	0.016	0.082	0.159	0.407	0.831

Table 2 The key locations on 10 cross-sections are compared between point-cloud data and the proposed mathematical model

Id	Line type	Top			Bottom			Mid-left-1			Mid-right-1		
		tm	om	dif	tm	om	dif	tm	om	dif	tm	om	dif
1	Transition curve	4460.3	4455	5.3	-934.9	-946.3	11.4	2729.2	2734.2	-5	2666.1	2665.7	0.4
2	Circular curve	4430.4	4427.7	2.7	-966.9	-971.3	4.4	2753.2	2755.2	-2	2643.4	2643.8	-0.4
3	Transition curve	4426.4	4425.3	1.1	-974.3	-972.5	-1.8	2776.8	2776.7	0.1	2622.8	2622.3	0.5
4	Straight line	4435.5	4432.3	3.2	-965.4	-963.1	-2.3	2811.3	2811.1	0.2	2588.9	2588.1	0.8
5	Straight line	4459.4	4451.7	7.7	-942.7	-941.2	-1.5	2839.9	2839.7	0.2	2562.1	2560.1	2
6	Straight line	4473.5	4469.2	4.3	-928.2	-924.2	-4	2834.4	2834.8	-0.4	2567.3	2565.2	2.1
7	Transition curve	4446.6	4444.5	2.1	-952.8	-947.1	-5.7	2849.7	2850.3	-0.6	2549.3	2549.4	-0.1
8	Circular curve	4451.3	4444.8	6.5	-949.2	-944.8	-4.4	2867.1	2866.8	0.3	2533.4	2532.8	0.6
9	Straight line	4461.4	4458.7	2.7	-935.2	-930.7	-4.5	2866	2869	-3	2530.8	2530.9	-0.1
10	Transition curve	4476.3	4473.4	2.9	-921.3	-917.9	-3.4	2852.8	2854.4	-1.6	2544.9	2545.6	-0.7

The analysis included the distance from the key locations extracted from the mathematical model to the tunnel centerline, denoted as tm, and the distance from the key point extracted from the point-cloud mathematical model to the centerline of the tunnel, denoted as om. The term dif is used to represent the difference between the two distances (Unit: mm)

Overall, our findings suggest that the model we constructed is a valuable tool for efficiently extracting key locations while meeting the required deviation standards.

4.4 Discussion

Generally, the method proposed in this paper offers several advantages. First, the method employs curve cylinders as tunnel models, which enables the rapid extraction of key locations and the quick verification of designed tunnel. Second, the rapid validation of design solutions supports the use of heuristic optimization algorithms during tunnel design, providing designers with efficient and flexible validation tools.

Nevertheless, the proposed method also has some limitations. First, the model construction process is time-consuming, which could negatively impact the overall efficiency of the design process. Second, as the method uses curve cylinders as proxy models, it may not be sensitive enough to capture irregular deformations in tunnels, therefore limiting its ability to accurately predict and validate design solutions in certain cases.

Future research can focus on improving the efficiency of model construction by introducing more efficient computational methods and optimization algorithms that can reduce the time required for model building. Furthermore, additional efforts can be made to enhance the method's sensitivity to irregular tunnel deformations by exploring more complex proxy models or incorporating additional input information to ensure more accurate modeling.

5 Conclusion

This paper introduces a mathematical model that accurately represents real metro tunnels and efficiently extracts key locations from point-cloud data using multiple cylinders. The findings of this study confirm that the constructed model serves as a valuable tool for effectively extracting key locations while adhering to the required deviation standards.

The proposed model offers several notable advantages. Firstly, it utilizes curved cylinders as tunnel models, enabling rapid extraction of key locations and efficient verification of the tunnel design. This allows for quick validation of design solutions, supporting the use of heuristic optimization algorithms during tunnel design and equipping designers with efficient and flexible validation tools.

However, it is essential to acknowledge the limitations of the proposed method. The process of constructing the model can be time-consuming, potentially impacting the overall design process efficiency. Additionally, relying on curved cylinders as proxy models, the method may have limitations

in accurately capturing irregular tunnel deformations, potentially resulting in inaccuracies when predicting and validating design solutions in specific cases.

Future research can focus on enhancing the efficiency of the model construction process by introducing more efficient computational methods and optimization algorithms that minimize the construction time. Furthermore, efforts can be made to improve the model's sensitivity to irregular tunnel deformations by exploring more intricate proxy models or incorporating additional input information to achieve more precise modeling.

Author contributions SC wrote the main manuscript text and wrote the code of the proposed method. JW prepared figures. JL and XW reviewed the manuscript.

Funding This work was supported in part by the National Natural Science Foundation of China [Grants 62176160, 61972265, 61732011 and 61772344], in part by the Guangdong Basic and Applied Basic Research Foundation [Grant 2022A1515010791], in part by the Natural Science Foundation of Guangdong Province of China [Grant 2020B1515310008], in part by the Educational Commission of Guangdong Province of China [Grant 2019KZDZX1007], in part by the Natural Science Foundation of Shenzhen [University Stability Support Program no. 20200804193857002], and in part by the Interdisciplinary Innovation Team of Shenzhen University. Finally, thanks go to Prof. Xizhao Wang for the supervisions and discussions during completing this paper.

Availability of data and materials Data will be made available on request.

Declarations

Competing interests The authors declare that they have no known competing financial interests or personal relationships that could have appeared to influence the work reported in this paper.

Open Access This article is licensed under a Creative Commons Attribution 4.0 International License, which permits use, sharing, adaptation, distribution and reproduction in any medium or format, as long as you give appropriate credit to the original author(s) and the source, provide a link to the Creative Commons licence, and indicate if changes were made. The images or other third party material in this article are included in the article's Creative Commons licence, unless indicated otherwise in a credit line to the material. If material is not included in the article's Creative Commons licence and your intended use is not permitted by statutory regulation or exceeds the permitted use, you will need to obtain permission directly from the copyright holder. To view a copy of this licence, visit <http://creativecommons.org/licenses/by/4.0/>.

References

1. Chen R, Zhang P, Wu H, Wang Z, Zhong Z (2019) Prediction of shield tunneling-induced ground settlement using machine learning techniques. *Front Struct Civ Eng* 13(6):1363–1378
2. Daotong L, Baofeng Y (2010) Common problems in metro track construction and their solutions. *J Railw Eng Soc* 27(04):97–100

3. Ding L, Yu H, Li H, Zhou C, Wu X, Yu M (2012) Safety risk identification system for metro construction on the basis of construction drawings. *Autom Constr* 27:120–137
4. Qian W, Qi T, Zhao Y, Le Y, Yi H (2019) Deformation characteristics and safety assessment of a high-speed railway induced by undercutting metro tunnel excavation. *J Rock Mech Geotech Eng* 11(1):88–98
5. Hu B, Li X, Huang D (2019) Safety risk analysis and protective control of existing pipelines affected by deep pit excavation in metro construction. *Model Simul Eng*. <https://doi.org/10.1155/2019/3643808>
6. Lan Q-P, Hong C, Lin H, Xue X-L (2015) Automatical extraction geometric feature lines in the tunnel from 3D point cloud. *Eng Surv Mapp* 24(10):1–4
7. Chen S, Wang H, Wang Q, Zhang G (2020) Fine-tuning of line and slope based on evolutionary mechanism. *Int J Mach Learn Cybern* 11:1–11
8. Chakeri H, Hasanpour R, Hindistan MA, Ünver B (2011) Analysis of interaction between tunnels in soft ground by 3D numerical modeling. *Bull Eng Geol Environ* 70(3):439–448
9. Van Gosliga R, Lindenbergh R, Pfeifer N (2006) Deformation analysis of a bored tunnel by means of terrestrial laser scanning. *Int Arch Photogramm Remote Sens Spatial Inf Sci* 36(5):167–172
10. Fekete S, Diederichs M, Lato M (2010) Geotechnical and operational applications for 3-dimensional laser scanning in drill and blast tunnels. *Tunn Undergr Space Technol* 25(5):614–628
11. Kai C, Da Z, Zhang Y (2013) Point cloud data processing method of cavity 3D laser scanner. *Acta Opt Sin* 33(8):0812003
12. Che E, Jung J, Olsen MJ (2019) Object recognition, segmentation, and classification of mobile laser scanning point clouds: a state of the art review. *Sensors* 19(4):810
13. Yuanrong H, Yuanmao Z, Huoping P, Jianzhi C (2016) Real three-dimensional modeling and application of complex construction based on the point cloud data. *Remote Sens Technol Appl* 31(6):1091–1099
14. Xue Y, Zhang S, Zhou M, Zhu H (2021) Novel SfM-DLT method for metro tunnel 3D reconstruction and visualization. *Undergr Space* 6(2):134–141
15. Björck Å (1990) Least squares methods. *Handb Numer Anal* 1:465–652
16. Miller SJ (2006) The method of least squares. *Math Dept Brown Univ* 8:1–7
17. Liu X, Fang Q, Zhang D (2018) Mechanical responses of existing tunnel due to new tunnelling below without clearance. *Tunn Undergr Space Technol* 80:44–52
18. Song S, Li S, Li L, Shi S, Zhou Z, Liu Z, Shang C, Sun H (2019) Model test study on vibration blasting of large cross-section tunnel with small clearance in horizontal stratified surrounding rock. *Tunn Undergr Space Technol* 92:103013
19. Yao L, Zhang S, Wang Z, Sun H, Chen Q, Gilbert K (2020) Metro gauge inspection system based on mobile laser scanning technology. *Surv Rev* 52(375):531–543
20. Chen W, Li D, Liu Y, Zhu Z, Huang Z, Yan J (2021) Development and application of a multi-sensor integration detection and analysis device for metro gauge and track geometric state. *AIP Adv*. <https://doi.org/10.1063/5.0053474>

Publisher's Note Springer Nature remains neutral with regard to jurisdictional claims in published maps and institutional affiliations.